Hollow-core Optical Fiber Gas Lasers (HOFGLAS): a review [Invited]

A. V. Vasudevan Nampoothiri,[1] Andrew M. Jones,[2] C. Fourcade-Dutin,[3] Chenchen Mao,[1] Neda Dadashzadeh,[2] Bastian Baumgart,[1] Y.Y. Wang,[3] M. Alharbi,[3] T. Bradley,[3] Neil Campbell,[1] F. Benabid,[3] Brian R. Washburn,[2] Kristan L. Corwin,[2] and Wolfgang Rudolph[1,*]

[1]Department of Physics and Astronomy, University of New Mexico, Albuquerque, New Mexico, USA
[2]Department of Physics, Kansas State University, 116 Cardwell Hall, Manhattan, Kansas 66506, USA
[3]GPPM, Physics department, University of Bath, Bath, UK & GPPMM, Xlim Research Institute, CNRS, Université de Limoges, France
**wrudolph@unm.edu*

Abstract: The development of hollow core photonic crystal fibers with low losses over a broad spectral region in the near IR enabled the demonstration of a novel laser type - Hollow-core Optical Fiber Gas Laser (HOFGLAS). The laser combines attractive features of fiber lasers such as compactness and long interaction length of pump and laser radiation with those of gas lasers such as the potential for high output power and narrow line width. This paper summarizes recent developments and describes the demonstration of C_2H_2 and HCN prototype lasers. Avenues to extend laser emission further into the IR are discussed.

OCIS codes: (140.4130) Molecular gas lasers; (060.3510) Lasers, fiber; (140.1340) Atomic gas lasers; (060.5295) Photonic crystal fibers; (140.3070) Infrared and far-infrared lasers.

References and links

1. E. Snitzer, "Optical maser action of Nd^{+3} in a barium crown glass," Phys. Rev. Lett. **7**(12), 444–446 (1961).
2. E. Stiles, "New developments in IPG fiber laser technology," in Proceedings of the 5th International Workshop on Fiber Lasers (2009).
3. Y. Kalisky and O. Kalisky, "The status of high-power lasers and their applications in the battlefield," Opt. Eng. **49**(9), 091003 (2010).
4. A. A. Ionin, "Electric Discharge CO Lasers," in *Gas Lasers* (CRC Press, 2007), pp. 201–237.
5. W. F. Krupke, R. J. Beach, V. K. Kanz, and S. A. Payne, "Resonance transition 795-nm rubidium laser," Opt. Lett. **28**(23), 2336–2338 (2003).
6. B. V. Zhdanov, T. Ehrenreich, and R. J. Knize, "Highly efficient optically pumped cesium vapor laser," Opt. Commun. **260**(2), 696–698 (2006).
7. J. Zweiback, A. Komashko, and W. F. Krupke, "Alkali vapor lasers," Proc. SPIE **7581**, 75810G, 75810G-5 (2010).
8. R. F. Cregan, B. J. Mangan, J. C. Knight, T. A. Birks, P. St. J. Russell, P. J. Roberts, and D. C. Allan, "Single-mode photonic band gap guidance of light in air," Science **285**(5433), 1537–1539 (1999).
9. F. Benabid, J. C. Knight, G. Antonopoulos, and P. St. J. Russell, "Stimulated Raman scattering in hydrogen-filled hollow-core photonic crystal fiber," Science **298**(5592), 399–402 (2002).
10. D. G. Ouzounov, F. R. Ahmad, D. Müller, N. Venkataraman, M. T. Gallagher, M. G. Thomas, J. Silcox, K. W. Koch, and A. L. Gaeta, "Generation of megawatt optical solitons in hollow-core photonic band-gap fibers," Science **301**(5640), 1702–1704 (2003).
11. K. Knabe, S. Wu, J. Lim, K. A. Tillman, P. S. Light, F. Couny, N. Wheeler, R. Thapa, A. M. Jones, J. W. Nicholson, B. R. Washburn, F. Benabid, and K. L. Corwin, "10 kHz accuracy of an optical frequency reference based on $^{12}C_2H_2$-filled large-core kagome photonic crystal fibers," Opt. Express **17**(18), 16017–16026 (2009).
12. F. Couny, F. Benabid, and O. Carraz, "Enhanced SRS in H_2 filled hollow core photonic crystal fiber by use of fiber Bragg grating," J. Opt. A, Pure Appl. Opt. **9**(2), 156–159 (2007).
13. F. Couny, F. Benabid, and P. S. Light, "Subwatt threshold cw Raman fiber-gas laser based on H_2-filled hollow-core photonic crystal fiber," Phys. Rev. Lett. **99**(14), 143903 (2007).
14. F. Couny, F. Benabid, P. J. Roberts, P. S. Light, and M. G. Raymer, "Generation and photonic guidance of multi-octave optical-frequency combs," Science **318**(5853), 1118–1121 (2007).

#167648 - $15.00 USD Received 30 Apr 2012; revised 6 Jun 2012; accepted 12 Jun 2012; published 20 Jun 2012

15. A. M. Jones, A. V. V. Nampoothiri, A. Ratanavis, T. Fiedler, N. V. Wheeler, F. Couny, R. Kadel, F. Benabid, B. R. Washburn, K. L. Corwin, and W. Rudolph, "Mid-infrared gas filled photonic crystal fiber laser based on population inversion," Opt. Express **19**(3), 2309–2316 (2011).
16. A. V. V. Nampoothiri, A. M. Jones, A. Ratanavis, R. Kadel, N. V. Wheeler, F. Couny, F. Benabid, B. R. Washburn, K. L. Corwin, and W. Rudolph, "Mid-IR laser emission form a C_2H_2 gas filled hollow core photonic crystal fiber," Proc. SPIE **7580**, 758001 (2010).
17. F. Benabid and P. J. Roberts, "Linear and nonlinear optical properties of hollow core photonic crystal fiber," J. Mod. Opt. **58**(2), 87–124 (2011).
18. F. Couny, F. Benabid, and P. S. Light, "Large-pitch kagome-structured hollow-core photonic crystal fiber," Opt. Lett. **31**(24), 3574–3576 (2006).
19. D. J. Richardson, J. Nilsson, and W. A. Clarkson, "High power fiber lasers: current status and future perspectives," J. Opt. Soc. Am. B **27**(11), B63–B92 (2010).
20. J. W. Dawson, M. J. Messerly, R. J. Beach, M. Y. Shverdin, E. A. Stappaerts, A. K. Sridharan, P. H. Pax, J. E. Heebner, C. W. Siders, and C. P. Barty, "Analysis of the scalability of diffraction-limited fiber lasers and amplifiers to high average power," Opt. Express **16**(17), 13240–13266 (2008).
21. C. Hensley, D. H. Broaddus, C. B. Schaffer, and A. L. Gaeta, "Photonic band-gap fiber gas cell fabricated using femtosecond micromachining," Opt. Express **15**(11), 6690–6695 (2007).
22. M. J. F. Digonnet, *Rare-Earth-Doped Fiber Lasers and Amplifiers* (Marcel Dekker, 2001).
23. X. Zhu and R. Jain, "Compact 2 W wavelength-tunable Er:ZBLAN mid-infrared fiber laser," Opt. Lett. **32**(16), 2381–2383 (2007).
24. S. Tokita, M. Murakami, S. Shimizu, M. Hashida, and S. Sakabe, "Liquid-cooled 24 W mid-infrared Er:ZBLAN fiber laser," Opt. Lett. **34**(20), 3062–3064 (2009).
25. H. Többen, "Room temperature CW fiber laser at 3.5 μm in Er^{3+}-doped ZBLAN glass," Electron. Lett. **28**(14), 1361–1362 (1992).
26. S. D. Jackson, "Continuous wave 2.9 μm dysprosium-doped fluoride fiber laser," Appl. Phys. Lett. **83**(7), 1316–1318 (2003).
27. J. Schneider, "Fluoride fiber laser operating at 3.9 μm," Electron. Lett. **31**(15), 1250–1251 (1995).
28. C. S. Kletecka, N. Campbell, C. R. Jones, J. W. Nicholson, and W. Rudolph, "Cascade lasing of molecular HBr in four micron region pumped by a Nd:YAG laser," IEEE J. Quantum Electron. **40**(10), 1471–1477 (2004).
29. A. Ratanavis, N. Campbell, A. V. V. Nampoothiri, and W. Rudolph, "Performance and spectral tuning of optically overtone pumped molecular lasers," IEEE J. Quantum Electron. **45**(5), 488–498 (2009).
30. J. E. McCord, A. A. Ionin, S. P. Phipps, P. G. Crowell, A. I. Lampson, J. K. McIver, A. J. W. Brown, and G. D. Hager, "Frequency-tunable optically pumped carbon monoxide laser," IEEE J. Quantum Electron. **36**(9), 1041–1052 (2000).
31. M. I. Buchwald, C. R. Jones, H. R. Fetterman, and H. R. Schlossberg, "Direct optically pumped multiwavelength CO_2 laser," Appl. Phys. Lett. **29**(5), 300–302 (1976).
32. D. Haberberger, S. Tochitsky, and C. Joshi, "Fifteen terawatt picosecond CO_2 laser system," Opt. Express **18**(17), 17865–17875 (2010).
33. B. Wellegehausen, "Optically pumped CW dimer lasers," IEEE J. Quantum Electron. **15**(10), 1108–1130 (1979).
34. R. L. Byer, R. L. Herbst, H. Kildal, and M. D. Levenson, "Optically pumped molecular iodine vapor-phase laser," Appl. Phys. Lett. **20**(11), 463–466 (1972).
35. J. B. Koffend and R. W. Field, "cw optically pumped molecular iodine laser," J. Appl. Phys. **48**(11), 4468–4472 (1977).
36. F. Désévédavy, G. Renversez, J. Troles, P. Houizot, L. Brilland, I. Vasilief, Q. Coulombier, N. Traynor, F. Smektala, and J. L. Adam, "Chalcogenide glass hollow core photonic crystal fibers," Opt. Mater. **32**(11), 1532–1539 (2010).
37. A. F. Kosolapov, A. D. Pryamikov, A. S. Biriukov, V. S. Shiryaev, M. S. Astapovich, G. E. Snopatin, V. G. Plotnichenko, M. F. Churbanov, and E. M. Dianov, "Demonstration of CO_2-laser power delivery through chalcogenide-glass fiber with negative-curvature hollow core," Opt. Express **19**(25), 25723–25728 (2011).
38. HITRAN database, *http://cfa-www.harvard.edu/HITRAN/*
39. GEISA, spectroscopic database, *http://ether.ipsl.jussieu.fr/etherTypo/?id=1293&L=0*
40. L. S. Rothman, C. P. Rinsland, A. Goldman, S. T. Massie, D. P. Edwards, J.-M. Flaud, A. Perrin, C. Camy-Peyret, V. Dana, J.-Y. Mandin, J. Schroeder, A. Mccann, R. R. Gamache, R. B. Wattson, K. Yoshino, K. V. Chance, K. W. Jucks, L. R. Brown, V. Nemtchinov, and P. Varanasi, "The Hitran Molecular Spectroscopic Database And Hawks (Hitran atmospheric workstation): 1996 edition," J. Quant. Spectrosc. Radiat. Transf. **60**(5), 665–710 (1998).
41. P. Russell, "Photonic crystal fibers," Science **299**(5605), 358–362 (2003).
42. Y. Y. Wang, N. V. Wheeler, F. Couny, P. J. Roberts, and F. Benabid, "Low loss broadband transmission in hypocycloid-core Kagome hollow-core photonic crystal fiber," Opt. Lett. **36**(5), 669–671 (2011).
43. A. M. Jones, C. Fourcade-Dutin, C. Mao, B. Baumgart, A. V. V. Nampoothiri, N. Campbell, Y. Wang, F. Benabid, W. Rudolph, B. R. Washburn, and K. L. Corwin, "Characterization of mid-infrared emissions from C_2H_2, CO, CO_2, and HCN-filled hollow fiber lasers," Proc. SPIE **8237**, 82373Y, 82373Y-10 (2012).
44. W. C. Swann and S. L. Gilbert, "Pressure-induced shift and broadening of 1510–1540-nm acetylene wavelength calibration lines," J. Opt. Soc. Am. B **17**(7), 1263–1270 (2000).

#167648 - $15.00 USD Received 30 Apr 2012; revised 6 Jun 2012; accepted 12 Jun 2012; published 20 Jun 2012

45. A. M. Smith, S. L. Coy, W. Klemperer, and K. K. Lehmann, "Fourier transform spectra of overtone bands of HCN from 5400 to 15100 cm^{-1}," J. Mol. Spectrosc. **134**(1), 134–153 (1989).
46. A. V. V. Nampoothiri, A. Ratanavis, N. Campbell, and W. Rudolph, "Molecular C_2H_2 and HCN lasers pumped by an optical parametric oscillator in the 1.5-μm band," Opt. Express **18**(3), 1946–1951 (2010).
47. J. Shephard, J. Jones, D. Hand, G. Bouwmans, J. Knight, P. Russell, and B. Mangan, "High energy nanosecond laser pulses delivered single-mode through hollow-core PBG fibers," Opt. Express **12**(4), 717–723 (2004).
48. B. C. Stuart, M. D. Feit, A. M. Rubenchik, B. W. Shore, and M. D. Perry, "Laser-induced damage in dielectrics with nanosecond to subpicosecond pulses," Phys. Rev. Lett. **74**(12), 2248–2251 (1995).
49. M. Herman, A. Campargue, M. I. El Idrissi, and J. Vander Auwera, "Vibrational spectroscopic database on acetylene, $X^1\Sigma_g^+$ ($^{12}C_2H_2$, $^{12}C_2D_2$, and $^{13}C_2H_2$)," J. Phys. Chem. Ref. Data **32**(3), 921–1361 (2003).
50. A. Maki, W. Quapp, S. Klee, G. Ch. Mellau, and S. Albert, "Infrared Transitions of $H^{12}C^{14}N$ and $H^{12}C^{15}N$ between 500 and 10 000 cm^{-1}," J. Mol. Spectrosc. **180**(2), 323–336 (1996).
51. K.-R. Sui, Y.-W. Shi, X.-L. Tang, X.-S. Zhu, K. Iwai, and M. Miyagi, "Optical properties of AgI/Ag infrared hollow fiber in the visible wavelength region," Opt. Lett. **33**(4), 318–320 (2008).
52. R. L. Abrams, "Coupling losses in hollow waveguide laser resonators," IEEE J. Quantum Electron. **8**(11), 838–843 (1972).
53. E. A. J. Marcatili and R. A. Schmeltzer, "Hollow metallic and dielectric waveguides for long distance optical transmission and lasers," Bell Syst. Tech. J. **43**, 1783–1809 (1964).
54. P. W. Smith, "A Waveguide Gas Laser," Appl. Phys. Lett. **19**(5), 132–134 (1971).
55. L. S. Rothman, R. L. Hawkins, R. B. Wattson, and R. R. Gamache, "Energy levels, intensities, and linewidths of atmospheric carbon dioxide bands," J. Quant. Spectrosc. Radiat. Transf. **48**(5-6), 537–566 (1992).
56. J. Han, K. Freel, and M. C. Heaven, "Rotational and vibrational energy transfer in vibrationally excited acetylene at energies near 6560 cm^{-1}," J. Chem. Phys. **135**(24), 244304 (2011).
57. A. Ratanavis, N. Campbell, and W. Rudolph, "Feasibility study of optically pumped molecular lasers with small quantum defect," Opt. Commun. **283**(6), 1075–1080 (2010).

1. Introduction

Since their invention in 1961 [1], fiber lasers have matured to a point where today 10 kW [2] can be obtained from a multi-diode pumped single fiber. Due to their compactness, ruggedness, and high conversion efficiencies, fiber laser systems have replaced conventional solid state and gas lasers in many areas of optical technology. Despite this remarkable progress, fiber lasers still lack the power levels obtainable with gas lasers, which can reach MW levels in chemical gas lasers [3]. More common gas lasers based on electrical discharges can also deliver extraordinarily high average (CW, >200 kW CO laser [4]) and pulsed optical output (~1.5 kJ [4]). Among other things, this is possible because of high damage thresholds and heat mitigation techniques specific to gases like for example gas flow. Very high quantum efficiency is achievable in optically pumped gas lasers (for example 98% in Rb [5]) and slope efficiencies of 81% have been demonstrated [6]. Diode-pumped alkali lasers (DPALs) have produced output powers as high as 145 W [7].

The advent of hollow-core photonic crystal fibers (HC-PCF) [8] and their ability to host gases for very long interaction lengths and within micro-scale modal areas [9] enabled new gas based nonlinear optical elements. Among nonlinear optical phenomena that have been demonstrated using HC-PCF are low damage-threshold stimulated Raman scattering [9], high energy soliton formation and guidance [10], precision saturated absorption spectroscopy [11], the development of a gas-filled fiber Raman laser [12,13], and multi-octave spanning Raman frequency combs [14].

The power scalability of fiber lasers is constrained by detrimental nonlinear optical processes and, ultimately, material damage in the solid core gain medium. Hence it is tempting to envision a laser concept without solid host where gain is provided by gases inside a hollow fiber core, thus taking advantage of both fiber and gas laser features. Such lasers can also capitalize on the broad spectral range of emission, from the UV to the IR, that can be covered by available gas active media. Owing to the nature of transitions in atomic and molecular gases the emission of such hybrid lasers is spectrally narrow even without additional bandwidth limiting elements.

Recently such an optically pumped 'Hollow-core Optical Fiber Gas Laser' (HOFGLAS) based on population inversion was demonstrated [15,16] with C_2H_2 as the gain medium in a ~40 μm hollow core photonic crystal fiber [17,18]. This new class of 'hybrid' fiber-gas lasers

#167648 - $15.00 USD Received 30 Apr 2012; revised 6 Jun 2012; accepted 12 Jun 2012; published 20 Jun 2012

holds the potential to generate diffraction limited beams in wavelength regions and at power levels beyond the fundamental limitations of rare-earth doped solid core fiber lasers. While solid core fiber and gas laser technologies have reached a high level of maturity as a result of intense research activities over the last 50 years, HOFGLAS technology today is just at its infancy and is confined to a few research laboratories. This paper reviews recent progress in optically pumped molecular gas-based HOFGLAS and discusses future directions of development.

In section 2, a comparison of solid core fiber lasers and HOFGLAS is made with an emphasis on power scaling and spectral coverage. Section 3 discusses selected properties of gas active media that can be used in HOFGLAS systems. Section 4 describes low loss hollow core photonic crystal fibers (HC-PCFs), a key component of HOFGLAS. Section 5 describes HOFGLAS prototypes with C_2H_2 and HCN as active gases in hollow core Kagome structured photonic crystal fibers. One of the current challenges HOFGLAS faces is the lack of practical low loss hollow fibers for wavelengths beyond 3.5 μm. Waveguide (capillary) based lasers can be used as a test bed for such HOFGLAS. These waveguide systems are considered in section 6 with CO and CO_2 as example active gas gain media. Modeling of HOFGLAS systems is discussed in section 7.

2. Spectral coverage and power limiting factors: solid core fiber lasers versus HOFGLAS

It is well known that nonlinear optical and thermal effects, such as Stimulated Brillouin Scattering (SBS), Stimulated Raman Scattering (SRS), thermal lensing, and material damage in silica ultimately limit the achievable output powers and energies of solid core fiber lasers [19,20]. Several of the rare-earth based systems operate already close to these fundamental limits. To a large extent the properties of the host material control the critical fiber parameters that determine the threshold for the onset of such processes. In a HOFGLAS the electromagnetic wave interacts only through an evanescent field with the fiber material (cladding). This field is typically at least an order of magnitude smaller than the peak field propagating in the hollow fiber core. The density of the active molecules (at a pressure of a few torr) in the core of HOFGLAS is too low (compared with a solid host) to contribute to SBS, SRS and optical damage.

Table 1 compares critical laser powers of solid core and HOFGLAS. For these examples we assumed 85% pump conversion of absorbed pump energy in a 10-m long fiber of diameter 40 μm at a pump wavelength of 1.5 μm.

Table 1. Comparison of critical powers / intensities for limiting processes in solid-core and gas-filled hollow-core fibers

Limiting factor	Solid core systems	HOFGLAS (5 torr gas filled)
SBS	50 W	10 MW
SRS	30 kW	600 MW
Thermal lens	50 kW	150 kW
Material damage	1.3 GW/cm^2	30 GW/cm^2

It is evident that in the case of HOFGLAS, the threshold for undesired nonlinear optical processes is orders of magnitude higher. Moreover, optical damage of the fiber occurs at power levels at least one order of magnitude larger than in solid-core fibers. This also suggests the possibility to generate comparatively larger energies in pulsed HOFGLAS systems. Moreover, the gas active media can be circulated in HC-PCFs [21], which should further increase the extractable power and energy from such systems.

Solid-core fiber lasers typically operate in the 1 μm to 2 μm wavelength region, see Fig. 1. The emission regions are determined by the active ions, for example Yb, Er, Pr, Tm, with which the silica core is doped [22]. By doping Er^{3+} (2.8 μm, 3 μm, 3.45 μm) [23–25], Dy^{3+} (2.9 μm) [26], Ho^{3+}(3.9 μm) [27] in fluorozirconate hosts, lasing between 2 μm and 4 μm has

#167648 - $15.00 USD Received 30 Apr 2012; revised 6 Jun 2012; accepted 12 Jun 2012; published 20 Jun 2012

been demonstrated. HOFGLAS can cover additional emission regions depending on the active gas used, cf. Fig. 1.

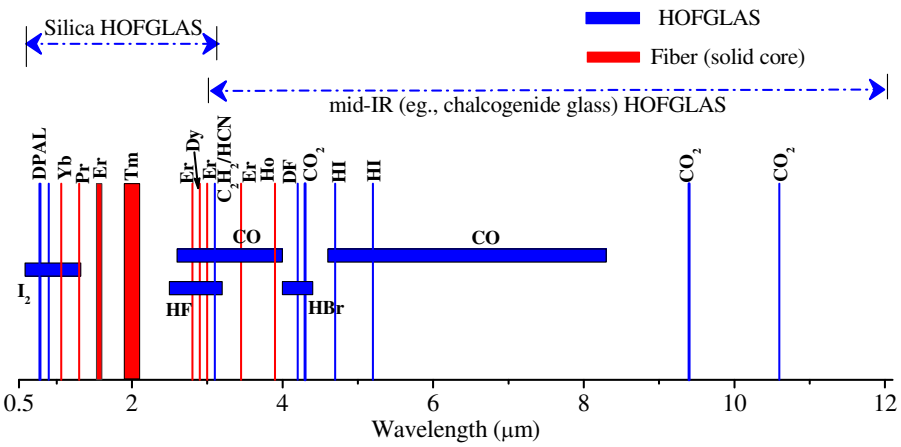

Fig. 1. Examples of laser emission from typical solid core fiber lasers with silica and fluorozirconate [22–27] hosts, and possible emission wavelengths in gases. The latter can principally be used in HOFGLAS with already available silica based HC-PCF [18] and TeAsSe (TAS) chalcogenide glass fibers [35,36]. The horizontal bars indicate many individual narrow lines.

Laser operation further into the IR utilizes rotation-vibration transitions in molecular gases, e.g., HBr, CO, CO_2 [28–32]. Emission in the VIS and UV typically relies on electronic transitions. Examples are dimer lasers [33] and I_2 [34,35] lasers.

In summary, HOFGLAS offers attractive features that can be exploited toward power scaling of fiber-based lasers and new wavelength regions further into the IR and possibly UV. This concept could be particularly useful to combine several mutual incoherent pump sources into one (coherent) laser beam.

3. HOFGLAS candidate gas media

Unlike solid state active media, the gain spectrum of molecular gases is comprised of narrow transitions that represent the rotation-vibration energy level structure of molecules. The line widths are determined by pressure and Doppler broadening and this also applies to atomic gases. For gas pressures of a few torr and below, the widths are $\Delta\nu \leq 500$ MHz and thus are much narrower than typical transitions of dopants in solid core fibers. Since the invention of the laser many optically pumped gas lasers have been demonstrated and studied using conventional gas cells. In principle, all these gases can be used in HOFGLAS provided the hollow core fiber is able to simultaneously guide pump and laser radiation with acceptable losses. Because of the much larger interaction lengths of pump and laser in HOFGLAS, gases whose cross-sections were too small for traditional lasers can be revisited, increasing the choice of active media. Table 2 lists examples of HOFGLAS candidate media and parameters.

#167648 - $15.00 USD Received 30 Apr 2012; revised 6 Jun 2012; accepted 12 Jun 2012; published 20 Jun 2012

Table 2. Candidate gas active media with pump and lasing parameters

Gas	Pump			Lasing		
	λ (μm)	Vibrational State	Cross-section (cm^2)	Vibrational Transition	Cross-section (cm^2)	λ (μm)
C_2H_2	1.52	$v_1 + v_3$	8.7×10^{-18}	$v_1 + v_3 \rightarrow v_1$	[(a)] 2.8×10^{-16}	3.1
HCN	1.53	$2v_3$	4.1×10^{-18}	$2v_3 \rightarrow v_3$	[(b)] 4×10^{-16}	3.1
HCN-CO	1.53	$2v_3$	4.1×10^{-18}	$v = 3 \rightarrow 1$	1.1×10^{-17}	2.36
HI	1.54	$v = 3$	2×10^{-19}	$v = 3 \rightarrow 2$	[(c)] 9.7×10^{-18}	4.76
CO	1.57	$v = 3$	1.5×10^{-20}	$v = 3 \rightarrow 1$	1.1×10^{-17}	2.36
CO_2	2.00	$(2v_1 + v_3)_{II}$	1.8×10^{-18}	$(2v_1 + v_3)_{II} \rightarrow 2v_1$	9.4×10^{-15}	4.3
HBr	1.97	$v = 2$	8.4×10^{-19}	$v = 2 \rightarrow 1$	2.7×10^{-16}	3.95
CO_2-N_2O	1.96	$(2v_1 + v_3)_I$	5.7×10^{-19}	$4v_1 \rightarrow v_1$	1.6×10^{-17}	2.6
				$4v_1 \rightarrow 2v_1$	4.4×10^{-16}	3.91
CO	2.33	$v = 2$	3.5×10^{-18}	$v = 2 \rightarrow 1$	1.7×10^{-15}	4.66
N_2O	1.98	$3v_1 + 2v_2$	1.4×10^{-19}	$3v_1 + 2v_2 \rightarrow v_1$	1.1×10^{-17}	2.66

The symbol v_i represents a vibrational normal mode of quantum number "i". Cross-sections are estimated using known Einstein coefficients [38–40] for the strongest R-band transition (according to Boltzmann's distribution at room temperature) and correspond to line shapes at low pressure (1 torr). In cases where data are not available, cross-section for a similar transition is used: [(a)] value for $v_3 \rightarrow 0$ transition, [(b)] value for $v_3 \rightarrow 0$, and [(c)] value for $v = 2 \rightarrow 1$ transition. The suffixes I and II denote different Fermi resonant sub-bands. HCN-CO and CO_2-N_2O are energy transfer systems, where the first molecule is optically pumped and transfers the energy to the second (active laser) molecule.

4. Low loss HC-PCF for HOFGLAS

Since their first demonstration [8] two major families of HC-PCFs have emerged. The first one is a photonic bandgap (PBG) guiding HC-PCF [41], and the second is an inhibited-coupling guiding HC-PCF [9]. The PBG guiding HC-PCF has potential of guiding light with ultra-low transmission loss; however, it exhibits a limited optical bandwidth. Furthermore, the strong power overlap of the guided mode with the silica core-surround limited the optical power handling of this type of HC-PCF. On the other hand, the inhibited-coupling guiding HC-PCF, which is coined Kagome-like HC-PCF, guides over much larger bandwidth but with higher transmission loss figures. The bandwidth and fiber loss can be tuned by the pitch and core shape of the fiber. Using this methodology, we have recently dramatically reduced the fiber loss to ~30 dB/km at 1550 nm by introducing the hypocycloid core shaped Kagome HC-PCF [42]. Finally, the guided mode of this fiber exhibits a much lower power overlap with the silica core-surround, making it an ideal host for high power gas lasers.

Figure 2 shows the transmission characteristics of different Kagome fibers over our spectral range of interest. Two types of hypocycloid-core Kagome HC-PCF were investigated. The first one consists of 3-ring (Fig. 2, left panel) cladding and the second one of 1-ring cladding (Fig. 2, right side panels). For both, different pitches and strut thickness were investigated. The loss of the Kagome fibers was characterized with cut-back measurements in the near-IR using a broadband illumination source and an optical spectrum analyzer to record transmission versus wavelength. For the 2.6 μm to 3.6 μm region, an optical parametric amplifier (OPA) was used as probe. The fiber loss measurements were performed by measuring the ratio of input to output power as a function of wavelength (OPA tuning) for a

#167648 - $15.00 USD Received 30 Apr 2012; revised 6 Jun 2012; accepted 12 Jun 2012; published 20 Jun 2012

single fiber length, and then cutting the fiber to a shorter length and repeating the ratio measurement. This was usually repeated so that two cut-back measurements were performed for each fiber. This process is lengthy and uncertainty arises due to its sensitivity to OPA power, mode and bandwidth while tuning. The error bars represent the repeatability of the measurement. The resulting curves represent the average of the fractional transmission through 1 m lengths based on two separate cutback measurements. For example, at 3.61 μm in the 42 μm pitch Kagome 1-ring fiber (Fig. 2, right bottom), the upper limit of the loss is 1.45 dB/m, as indicated by the error bar.

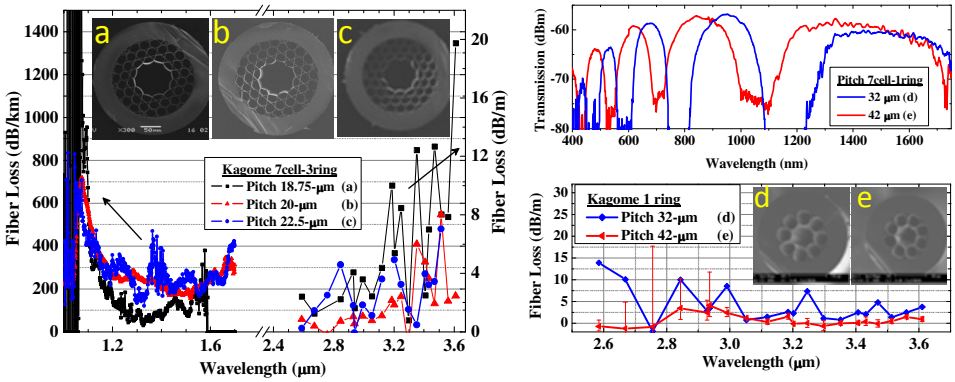

Fig. 2. (a-c): Kagome fibers having hypocycloid core with 3 cladding rings and 7 cell defects with pitches of 18.75 μm, 20 μm, and 22.5 μm and core diameters of 85-93.75, 87.5 – 92.5, and 85-93.75 μm; (d-e): Kagome fibers with hypocycloid core structure having 1 cladding ring with pitches of 32 μm and 42 μm and core sizes of 58 μm and 64 μm respectively. (left) fiber loss vs wavelength in the near and mid-IR for 3 ring hypocycloid fibers (a)-(c). (Right top) Transmission of 1 ring Kagome hypocycloid core fibers in the near IR. For reference, the loss in 42 μm pitch fiber (red) is measured to be 5 dB/m at 1.50 μm wavelength. (Right bottom) mid-IR loss of 1 ring Kagome hypocycloid core fibers measured with the OPA. Error bars are generated from repeatability of 2 cut-backs of fiber length 0.8 and 2.0 m.

Both types (3-ring and 1-ring) of fibers have extremely small loss in the 3-μm region while still maintaining acceptable loss (~< 5dB/m, with a minimum reaching 30 dB/km) in potential pump wavelength regions at ~1.5 μm. The hypocycloid structure exhibits a larger wavelength region where losses are below 1.5 dB/m and its fiber properties can be tuned for particular target lasing and pump wavelengths, making this breed of hollow fibers ideal for HOFGLAS applications.

5. Representative HOFGLAS systems: C_2H_2 and HCN

The central element of a HOFGLAS is a hollow core fiber (HCF) terminated in small vacuum chambers for gas filling and optical windows, see Fig. 3.

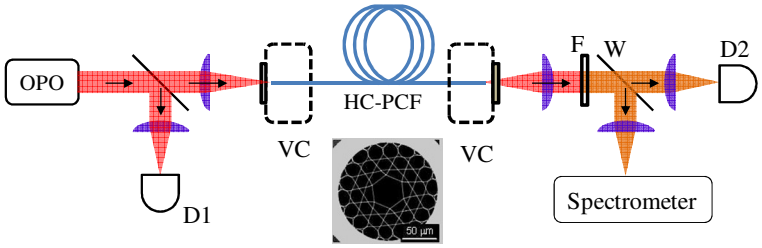

Fig. 3. Schematic diagram of a HOFGLAS operating in the mid IR spectral region. HC-PCF: for example a Kagome circular core structured hollow core photonic crystal fiber of core diameter ~40 μm and cross section as shown, VC- vacuum chambers filled with active gas. D1, D2: detectors, F- germanium filter to separate residual pump from laser. W is an uncoated CaF_2 window.

#167648 - $15.00 USD Received 30 Apr 2012; revised 6 Jun 2012; accepted 12 Jun 2012; published 20 Jun 2012

In principle, the vacuum chamber can be removed and the fiber closed by optically welding windows to both fiber ends. The first HOFGLAS demonstration [15,16] used a pulsed optical parametric oscillator (OPO) as a pump source. The pump is coupled into the gas filled fiber from one end, laser output is observed at the other end. Here we review two representative HOFGLAS systems: (i) $^{12}C_2H_2$ [15,16], and (ii) $H^{12}C^{14}N$ [43]. Both C_2H_2 and HCN have strong absorption in the 1.52-1.55 μm region [44,45] and hence are well suited for optical pumping in the fiber optic communication C-band, for example, with Erbium fiber lasers. C_2H_2 and HCN have been shown to lase in the mid-IR when optically pumped at 1.5 μm in conventional gas cells [46].

Both HOFGLAS systems were pumped with nanosecond pulses from an OPO or OPA. The pulse, tuned to resonance with a particular absorption transition of the active gas, was coupled to the fiber using appropriate optics. The pump pulse fluence incident on the fiber was kept well below the damage threshold of the cladding, which was estimated to be about 42 J/cm^2 based on measurements [47] for this class of fibers with 8-ns pulses, and scaling to 1-ns pulses used in our measurements assuming a square root dependence [48] of the damage fluence with respect to pulse width. The gain was high enough to generate lasing with a single pass of the pump, avoiding the need for external mirrors. Suitable filters were used to separate the transmitted pump light from the laser pulses exiting the fiber. The laser output was recorded using a fast detector and the laser spectrum was recorded using a near infrared scanning spectrometer. For both systems, the experiments were carried out at room temperature.

5.1. C_2H_2 HOFGLAS

The observed C_2H_2 laser spectrum when pumped at 1.521 μm (R(7), $v_1 + v_3$ transition) with 4 ns pulses is shown in Fig. 4(a) together with a simplified energy level diagram. In principle, C_2H_2 can be pumped on any of the rotation-vibration transitions from the ground state to the $v_1 + v_3$ vibrational state, and lasing occurs from the upper pumped rotational level. Typically, a pump wavelength is chosen close to the maximum absorption. The gain of such lasers is very high and its first demonstration was possible with a fiber exhibiting losses of 20 dB/m at the lasing wavelength and 0.75 dB/m losses for the pump (fiber A) [15,16]. The laser spectrum contains two peaks corresponding to R(7) and P(9) transition [49] from the pumped state. Pump laser thresholds as low as 200 nJ were observed.

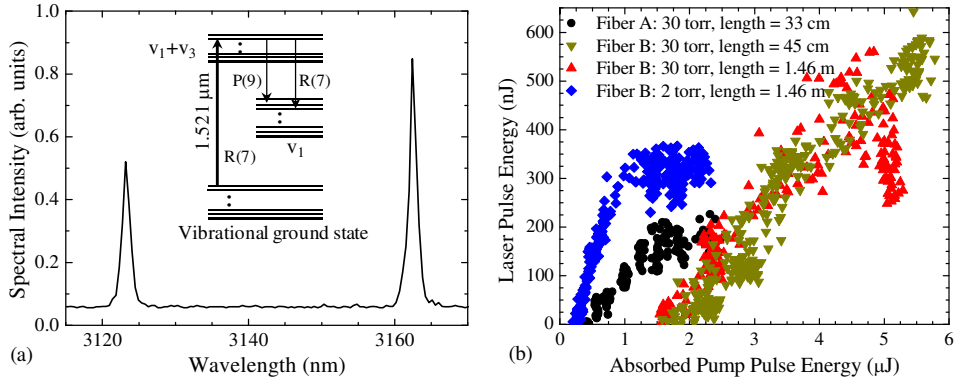

Fig. 4. (a) Spectrum of a C_2H_2 (7 Torr) filled HOFGLAS and energy level diagram of C_2H_2 showing the observed lasing transitions. The group of horizontal lines for each vibrational state are to indicate the manifold of rotational states. P(J), R(J) refers to transitions J-1 → J and J + 1 → J respectively, where J is the rotational quantum number of the lower vibrational state. A 40-μm diameter Kagome fiber (23 μm pitch) with a length of 165 cm was used. The pump energy was 1.6 μJ and the OPO pump bandwidth was ~3.5 GHz. (b) Total laser pulse energy of a C_2H_2 HOFGLAS as a function of absorbed pump energy for two different fibers, see text, and selected gas pressures. The P(13) transition to the ($v_1 + v_3$) state was pumped with a 1-ns pulse.

#167648 - $15.00 USD Received 30 Apr 2012; revised 6 Jun 2012; accepted 12 Jun 2012; published 20 Jun 2012

Figure 4(b) shows the laser output energy (sum of the two spectral components) as a function of the absorbed pump energy obtained with two different fibers (fiber A and B). Fiber B exhibited losses of 5 dB/m and 0.12 dB/m for the laser and pump wavelength, respectively. The P(13) absorption transition was excited with 1-ns pump pulses and the two lasing components shown in Fig. 4(a) are shifted to 3114.6 nm and 3172.4 nm corresponding to the R(11) and P(13) transitions, respectively.

At low pressures, the output shows onset of saturation as the pump energy is increased. Not surprisingly, the laser efficiency increased in switching from the higher-loss ~40-μm core Kagome fiber (fiber A) to the lower-loss ~85-μm core fiber (fiber B). However, the threshold also increased. While the loss per unit length is reduced by a factor of ~30, the core diameter is increased by a factor of two, reducing the fluence by a factor of ~4, which results in larger threshold pump energies. Changing the length of the low loss Kagome fiber from 1.46 m to 45 cm does not have significant impact on the laser threshold or optical-to-optical efficiency. For the low-loss fiber a maximum efficiency of 27% was observed for a pressure of 2 torr. This is close to the theoretical limit of this system of 33% determined by simultaneous saturation of pump and lasing transitions.

5.2. HCN HOFGLAS

The molecules HCN and C_2H_2 have similar energy levels and similar HOFGLAS behavior is expected. Indeed, pumping the P(10), $2\nu_3$ transition [45] of HCN at 1541 nm using 1 ns pulses results in a spectrum similar to what is shown in Fig. 4(a) for both fiber A and B. The two emission lines (now at 3091 nm and 3147 nm) also originate at the upper pump level and correspond to the R(8) and P(10) transition between the $J = 9$, $2\nu_3$ excited state and the $J = 8$ and $J = 10$, ν_3 states [50]. The HCN laser spectrum in the short, low-loss fiber indicates that the longer wavelength P-branch transition is favored over the shorter wavelength R-branch transition, most likely due to wavelength-dependent absorption in the fiber.

Figure 5(a) shows the mid-IR laser pulse energy as a function of the absorbed pump pulse energy for an HCN pressure of 19 torr. The absorbed pump pulse energy threshold was 1 μJ with an optical-to-optical efficiency of 0.02%. The much reduced efficiency (as compared with acetylene) may be due to poor OPA performance in this experiment. Figure 5(b) shows the maximum observed laser pulse energy as a function of absorbed pump pulse energy for various pressures of HCN gas contained within 45 cm of fiber B.

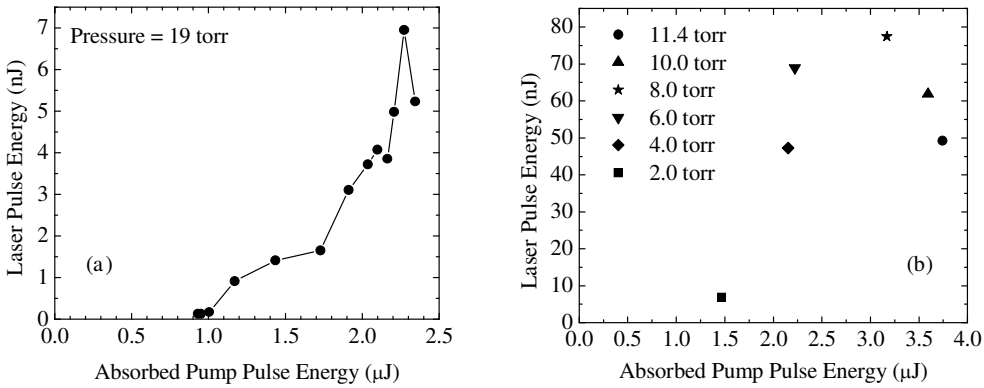

Fig. 5. (a) Laser pulse energy as a function of absorbed pump pulse energy for 33-cm long high-loss fiber 'A' filled with 19 torr of HCN gas, (b) maximum laser pulse energy as a function of absorbed pump pulse energy for various pressures of HCN gas contained in 45 cm long low-loss fiber 'B'.

For the low-loss fiber B, the maximum laser pulse energy observed is ~80 nJ and occurs at an HCN pressure of 8 torr. This is a factor of 10 higher than the maximum laser pulse energy

#167648 - $15.00 USD Received 30 Apr 2012; revised 6 Jun 2012; accepted 12 Jun 2012; published 20 Jun 2012

observed in fiber A, most likely due to the lower loss in fiber B. Still, the HCN-filled laser produced a factor 10 lower laser pulse energy than that produced by the acetylene laser at 30 torr in the same fiber, cf. Fig. 4(b).

6. Hollow Waveguides – alternate option for mid-IR

While successful mid-IR operation of HOFGLAS has been demonstrated [15,16], extension of the laser emission beyond 3.5 μm is not possible with silica glass fibers due to material absorption. Hollow fibers based on chalcogenide glass with guiding properties in this region are on the horizon [36,37] and will be of interest for HOFGLAS if they can also provide low loss guiding for the needed pump wavelengths. Currently available silver coated glass capillaries [51] can serve as surrogates to study lasing of gases in the mid-IR and beyond.

6.1. Guiding in capillary waveguides

Under optimal coupling, the free-space TEM00 mode couples to the EH11 waveguide mode with ~98% efficiency [52]. The waveguide power loss for the dominant EH11 mode is given by [53],

$$\alpha = \frac{1}{2}\left(\frac{2.405}{\pi}\right)^2 \frac{\lambda^2}{a^3}\,\mathrm{Re}\left(\frac{1}{2}\frac{n^2+1}{\sqrt{n^2-1}}\right), \qquad (1)$$

where λ is the wavelength, a is the radius of the waveguide, and n is the complex refractive index of the material of the inner-wall coating (for example, silver). Figure 6 compares the loss of a 500-μm and a 40-μm diameter, silver coated capillary to that of a HCF (40-μm diameter silica Kagome fiber). While silica based HCFs of comparable diameter show clear advantages in the near IR up to about 3.5 μm, they cannot be used at longer wavelengths unlike coated capillaries.

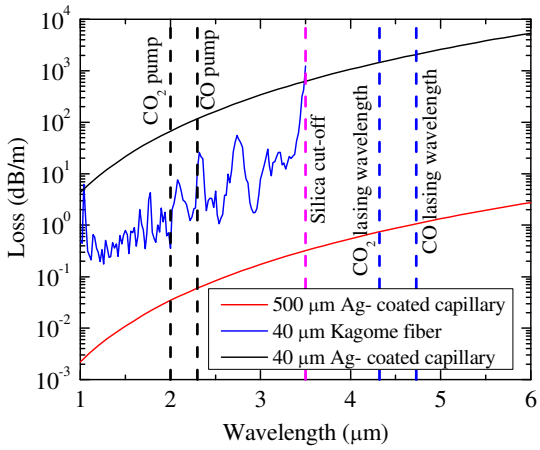

Fig. 6. Propagation losses for silver (Ag) coated capillaries [from Eq. (1)] and calculated losses for a Kagome fiber [8,10–12,42] as a function of wavelength. Possible pump and laser wavelengths for CO and CO_2 active media are also indicated.

6.2. CO and CO_2-filled waveguide lasers

The basic layout of a gas – capillary laser [54] is the same as shown in Fig. 3 except that the glass capillary replaces the fiber, see Fig. 7. In our realization we pumped the v = 0 → 2, R(7) and $2v_1 + v_3$, R (22) transitions of CO and CO_2, respectively at 2.33 μm and 2.00 μm using 5-ns pulses from an OPO. Both the lasers were operated at room temperature. The laser threshold was about 40 μJ of absorbed pump energy for CO_2 and ~5 μJ in case of CO for typical gas pressures of 50 torr.

#167648 - $15.00 USD Received 30 Apr 2012; revised 6 Jun 2012; accepted 12 Jun 2012; published 20 Jun 2012

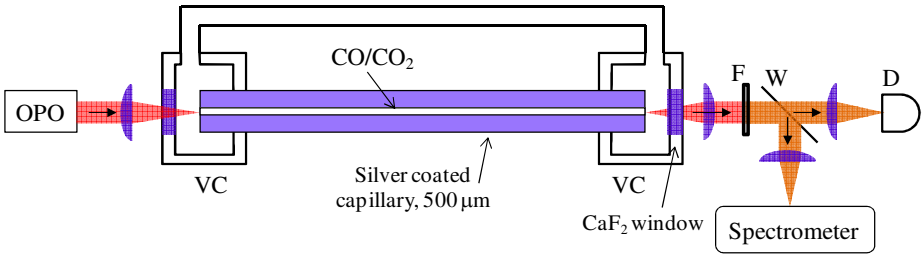

Fig. 7. Experimental setup of an optically pumped mid-IR CO and CO_2 capillary waveguide laser. VC- vacuum chambers filled with active gas, F- filter to suppress pump beam, W- uncoated CaF_2 window, D- detector. The length of the capillary was 1.5 m.

From Fig. 6, the estimated losses for the pump and laser radiation in the waveguide are about 0.04 dB/m and 0.9 dB/m, respectively.

Figure 8(a) shows the spectrum of the mid-IR laser pulses generated from the CO_2-filled (5 torr) waveguide laser together with an energy level diagram showing relevant transitions. From the spectroscopic constants of the molecule [55], our preliminary assessment is that the peak near 4.30 μm corresponds to the expected R(22) transition between the terminal pump state and the lower lying $J = 22$, $2v_1$ state, while the peak near 4.37 μm likely corresponds to the transition from $J = 19$, $2v_1 + v_3 \rightarrow J = 20$, $2v_1$; the $J = 19$ in the upper state being populated during relaxation from the initially populated $J = 23$ pump level. A very similar spectrum was observed when CO (50 torr) was pumped on its R(7) transition. Two laser components were observed at 4.67 μm and 4.78 μm corresponding to the R(7) and P(6), v = 2→1 transition.

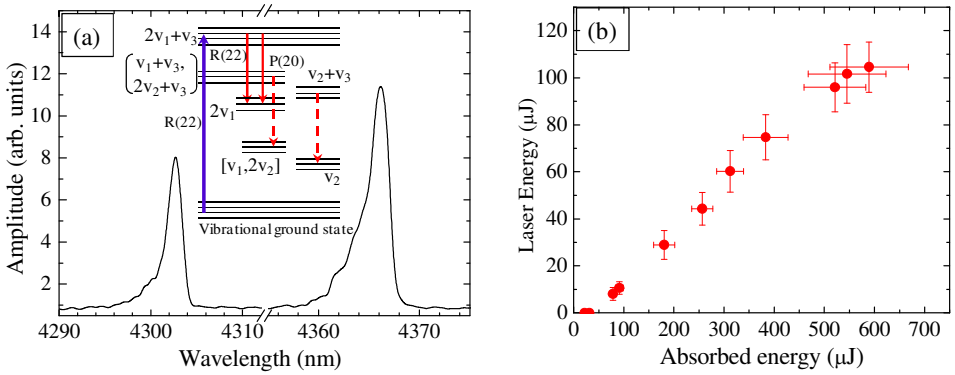

Fig. 8. (a) Observed lasing transitions from the optically pumped CO_2 waveguide laser, and energy level diagram showing pump and lasing transitions. Solid red arrows indicate lasing transitions, dashed arrows indicate other possible transitions. The levels in square brackets denote Fermi resonant states, (b) CO_2 waveguide laser energy as a function of absorbed pump energy at a pressure of 100 torr. The lasing threshold is about 40 μJ.

Figure 8(b) shows the laser pulse energy as a function of absorbed pump pulse energy for the waveguide CO_2 laser measured for a gas pressure of 100 torr. A maximum laser pulse energy of about 105 μJ corresponding to a laser efficiency of ~18% is observed.

7. Modeling of HOFGLAS

Modeling pulsed HOFGLAS requires propagating the pump pulse and emerging laser pulse through the gas filled fiber. To this end, the fiber is divided into slices of length ΔL. In each slice a set of rate equations for the occupation numbers of relevant gas energy levels and the laser and pump fluence is solved. After accounting for the linear fiber losses the obtained pump and laser pulse serve as input for the next slice. Molecular line broadening and

#167648 - $15.00 USD Received 30 Apr 2012; revised 6 Jun 2012; accepted 12 Jun 2012; published 20 Jun 2012

relaxation kinetics are controlled by collisions with other active gas and buffer gas molecules and such processes must be modeled to explain optically pumped gas lasers in quantitative detail, see for example [29]. Figure 9(a) shows a simplified energy level diagram to be used here for a qualitative understanding of C_2H_2 HOFGLAS features.

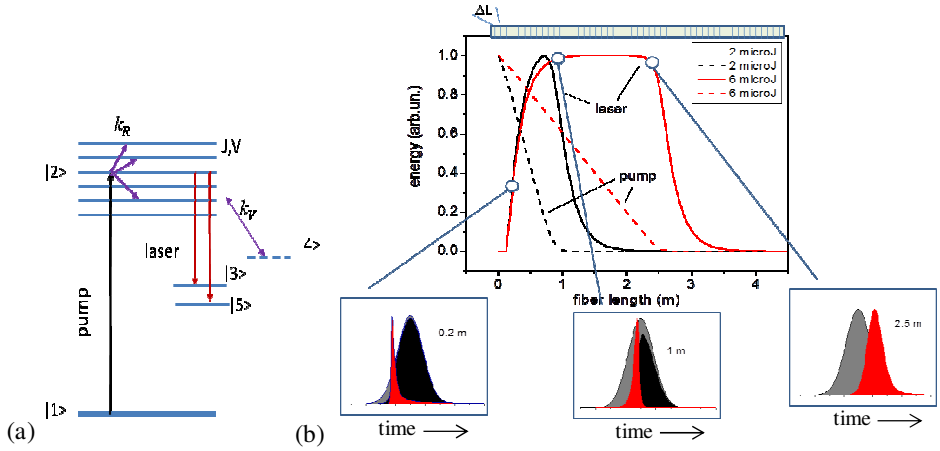

Fig. 9. (a) Five-level energy diagram of C_2H_2 showing the pump transition, two possible laser transitions and rotational (k_R) and vibrational (k_V) relaxation rates that determine the total removal rate of population from the upper laser level. A total removal rate of k_{tot} ~1.3 10^{-15} $m^{-3}s^{-1}$ [56] was used in the simulations and the fiber loss for the pump was neglected. (b) Schematic diagram of the sliced fiber, and calculated pump and laser pulse energies (normalized) as a function of the position in the fiber for two different pump pulse energies. The three bottom subplots show the calculated temporal evolution of pump (gray), laser (red), and depleted pump (black) pulses at three different positions in the fiber (5 ns pump pulse duration, 20 dB/m laser loss).

Depending on the actual gas, fiber and pump parameters the laser pulse starts somewhat delayed with respect to the absorbed pump. If the fiber extends beyond the point of complete absorption of the pump the laser pulse energy decreases due to the linear fiber losses. An optimum fiber length can thus be expected for given pump energy and fiber loss. If the fiber is short sufficiently large pump energy can saturate the absorption transition completely and increase in pump energy will not change the laser energy much. Figure 10(a) shows the laser energy as a function of fiber length for a high and a low-loss fiber and different fiber diameters. Figure 10(b) shows the laser energy versus fiber length for different gas pressure.

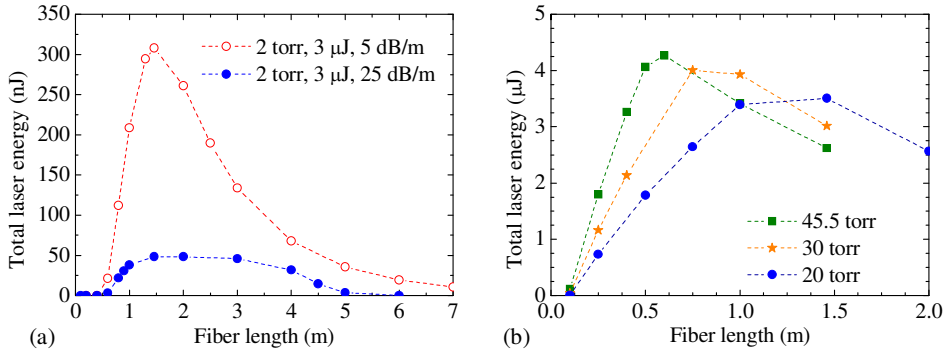

Fig. 10. (a) Laser energy as a function of fiber length for 20dB/m and 5 dB/m losses at the laser wavelength and fiber diameters of 85 μm and 45 μm, respectively as predicted by the model. (b) Calculated laser energy as a function of the fiber length at different pressures in the low loss fiber. The incident pump energy was constant (30 μJ) and the pump pulse duration was 1 ns. The pump laser was in resonance with the P(13) transition.

#167648 - $15.00 USD Received 30 Apr 2012; revised 6 Jun 2012; accepted 12 Jun 2012; published 20 Jun 2012

Longer fibers are advantageous for lower gas pressure. If the pump fluence is large enough to saturate the absorption transition there is a region of fiber length over which the laser output does not change; gain and linear fiber loss are equal. If the pump cannot saturate the transition a distinct optimum fiber length exists at which gain equals loss.

The gas pressure p controls the number density of active molecules, the absorption and lasing cross sections ($\sigma \propto 1/p$ in the region where pressure broadening dominates Doppler broadening) as well as the relaxation out of the upper laser level, which is expected to affect laser threshold and efficiency. This is exemplified in Fig. 11. The increase in laser threshold and decrease in slope efficiency with increasing gas pressure is qualitatively similar to what was measured; cf. Fig. 4(b). Neglecting population removal from the upper laser level, the maximum possible efficiency is ~33% and corresponds to the situation where the $1 \rightarrow 2$ pump transitions and the two gain transitions, $2 \rightarrow 3$ and $2 \rightarrow 5$ are completely saturated, cf. Fig. 9.

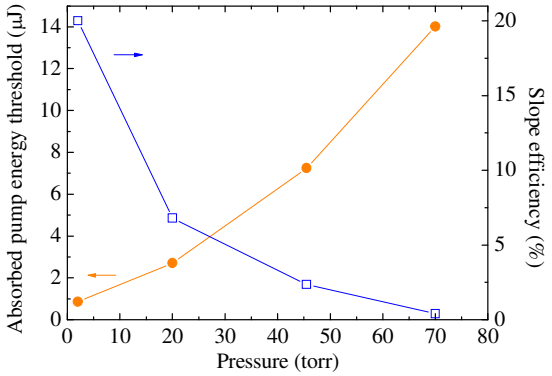

Fig. 11. Calculated pump energy at laser threshold and slope efficiency using the maximum absorbed energy from experiment as a function of gas pressure for a 1.46- m long fiber and 5 dB/m losses for the laser.

For a better quantitative agreement of simulation and experiment a more comprehensive gas model is necessary, taking into account additional energy levels and relaxation processes. In addition the mode profile in the HCF must be considered.

8. Summary

Recent progress in the development of hollow-core photonic crystal fibers with low propagation loss in broad frequency regions in the near and mid IR enabled a new class of lasers where the active medium is a gas inside the hollow core, which is optically pumped. Prototypes of such lasers dubbed HOFGLAS (Hollow-core Optical Fiber Gas Laser), were first demonstrated with C_2H_2 and HCN as active gases, and operated in pulsed mode using a nanosecond pump pulse. The gain in the 3-micron region is large enough so that a single path of the pump results in lasing without external cavity. The laser output is intrinsically spectrally narrow because of the small transition line width of molecular gases at a pressure of a few Torr. Pump energy thresholds are as low as a few hundred nJ. Because only the evanescent field of the guided pump and laser mode interacts with the host material undesired nonlinear optical effects like stimulated Brillouin scattering (SBS) and damage are expected to occur at much higher energy and power levels compared to solid core fibers. Extension of the wavelength region further into the IR seems possible with recent developments in hollow-core chalcogenic fibers. Corresponding gas media in coated glass capillaries, for example CO and CO_2, showed lasing in the 4-micron region when pulse pumped at about 2 μm. While currently still in its infancy HOFGLAS is an attractive new laser concept for single frequency, high-power emission in the IR spectral region and beyond. While the present HOGLASs operate in pulsed mode, cw operation seems possible with the right combination of active gas

#167648 - $15.00 USD Received 30 Apr 2012; revised 6 Jun 2012; accepted 12 Jun 2012; published 20 Jun 2012

and pump laser. One concept involves lasing of HCN with small Stokes shift when pumped with a C-band source [57]. Another possibility is I_2 pumped at 532 nm, which has produced lasing using conventional gas cells three decades ago [35].

Acknowledgments

The authors acknowledge funding from AFOSR FA9550-10-1-0515, JTO/ARO W911NF-05-1-0507, ARO W911NF-08-1-0332 and W911NF-10-C-0034. We are grateful to Tobias Fiedler for help with the capillary laser.

#167648 - $15.00 USD Received 30 Apr 2012; revised 6 Jun 2012; accepted 12 Jun 2012; published 20 Jun 2012